



Research Article

# Characterization methods of nickel nano-particles obtained by the ex-solution process on the surface of Pr, Ni-doped SrTiO<sub>3</sub> perovskite ceramics

B. Kamecki<sup>1</sup> · T. Miruszewski<sup>1</sup> · K. Górnicka<sup>1</sup> · T. Klimczuk<sup>1</sup> · J. Karczewski<sup>1</sup> 

© The Author(s) 2019 **OPEN**

## Abstract

In this paper, a novel electrode material based on Pr, Ni co-doped strontium titanate (Sr<sub>0.7</sub>Pr<sub>0.3</sub>)<sub>x</sub>Ti<sub>1-y</sub>Ni<sub>y</sub>O<sub>3</sub> with constant amount of 30% praseodymium dopant, different amount of nickel (y = 0.06 and y = 0.10) and additional nonstoichiometry in Sr-site (x = 1; x = 0.9 and x = 0.8) was investigated as fuel electrode for SOEC devices. A porous ceramics were prepared by solid-state reaction method. X-ray diffraction measurements revealed single phase materials with perovskite structure. Ex-solution method makes the grain surface covered by nickel nanoparticles. The influence of nickel amount, non-stoichiometry, synthesis and reduction conditions on formation of nanoparticles was investigated. Size, distribution and ability to agglomeration of Ni nanoparticles were analyzed by the scanning electron microscopy. The quantity of ex-soluted Ni particles was calculated from magnetization measurement. The total electrical conductivity of samples was measured by DC 4-wire method in the range of 100–800 °C at different atmospheres. Electrical measurements showed total electrical conductivity higher than 10 S cm<sup>-1</sup> in a wide temperature range. All obtained results confirmed that analyzed donor and acceptor co-doped SrTiO<sub>3</sub> materials with Ni nanoparticles after ex-solution process should be a good candidate to improve a catalysis process on fuel electrode surface.

**Keywords** SOFC · SOEC electrodes · Doped-strontium titanate · Electrical conductivity · Perovskites · Redox cycles · ex-solution · Nickel nanoparticles

## 1 Introduction

During the last 20 years, it has been reported, that the reversible solid oxide cells (SOC) are a potential technology to obtain an energy in different forms. These devices, which can be used for produce electricity, are called Solid Oxide Fuel Cells (SOFCs). The SOC which can be also used for hydrogen or synthetic fuel production is called Solid Oxide Electrolysis Cells (SOECs). Solid Oxide Electrolysis Cell (SOEC) is an electrochemical device that can convert molecular H<sub>2</sub>O in steam form or/and CO<sub>2</sub> into H<sub>2</sub> or/and CO. The operational temperature of SOEC is very high and is in the range of 800–1000 °C. It is caused, by the low ionic

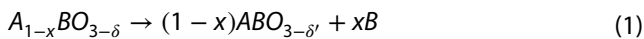
conductivity of used electrolyte at lower temperatures and the low efficiency of electrochemical processes [1–3].

The electrocatalytic activity of electrode materials in SOFC/SOEC has a great effect on the electrochemical performance of whole device. The electrochemical resistance related to the rate of the redox reactions (oxidation and reduction) which takes place on the triple phase boundary (TPB) points can be overcome *i.a.* by the introducing of metallic particles [4]. One of these methods is to incorporate the metal as a dopant into the material sublattice during the synthesis in air, which can be then exsolved at the grain-surface in the metallic form of catalytically active metal nanoparticles under reducing conditions. It was recently shown that electro-catalytic nanoparticles

✉ J. Karczewski, jakub.karczewski@pg.edu.pl | <sup>1</sup>Solid State Physics Department, Faculty of Applied Physics and Mathematics, Gdańsk University of Technology, ul. G. Narutowicza 11/12, 80-233 Gdańsk, Poland.

can be produced in oxide anodes by incorporating Ni, Co, Cu, Fe, Pd into perovskite oxide [5, 6]. These catalytically active nanoparticles can be incorporated back into the substrate to form a homogeneous ceramic where the exsolved specie is again a dopant into the sublattice [7–10].

The stoichiometry of perovskites plays a crucial role in case of metallic nanoparticles exsolution process. For stoichiometric  $ABO_3$  perovskite compounds ( $A/B = 1$ ) only a limited numbers of reducible and catalytically active ions, *i.e.*  $Ru^{2+}$ ,  $Rh^{4+}$ ,  $Pt^{4+}$ ,  $Pd^{4+}$  or  $Ni^{2+}$  can be found [6, 11, 12]. Moreover, in case of these type of dopants, exsolution takes place rather in the bulk than on the surface of material grains [13]. It was reported [7, 9, 14] that the A-site nonstoichiometry ( $A/B < 1$ ) has a great influence on the exsolution process in perovskites with a harder-to-reduce cations. In this type of compounds, the exsolution process can be described as Eq. (1):



As can be seen, the amount of the metal particles in the exsolution process is proportional to the nonstoichiometry value in cationic A-site ( $x$  in Eq. (1)). Thus, the nonstoichiometry should be favorable in the exsolution process. The influence of A-site nonstoichiometry on the structure and charge transport properties was previously shown for  $Sr(Ti,Nb)O_3$  [15] ( $La,Sr)(Ti,Ni)O_3$  [7] or  $Sr(Ti,Nb,Ni)O_3$  [9] systems.

In this work, Pr and Ni co-doped strontium titanate samples:  $(Sr_{0.7}Pr_{0.3})_{1-x}Ti_{1-y}Ni_yO_3$  with constant amount of praseodymium dopant, different amount of nickel and additional nonstoichiometry in Sr-site were investigated. The aim of this work was to check the influence of two different combinations on the properties of material: (a) different amount of the nickel with a constant nonstoichiometry level in Sr-site; and (b) the different nonstoichiometry level with a constant Ni dopant amount in a titanium sublattice. In our work, the 30 mol% of praseodymium donor dopant was chosen according to the previous literature reports [16, 17]. The nickel dopant into the titanium sublattice and Sr-site nonstoichiometry was introduced in order to improve the catalytic activity of the material and in order to introduce the Ni-metallic particles at a grains surface in exsolution process. The structure, redox cycles stability and general magnetic and electrical properties of sintered ceramics were investigated in regards to SOEC cathode application.

## 2 Experimental

The  $(Sr_{0.7}Pr_{0.3})_xTi_{1-y}Ni_yO_3$  ceramic sample has been prepared via solid state synthesis method. Non-stoichiometry in Sr-sublattice  $x = (1; 0.9; 0.8)$  and Ni dopant concentration

$y = 0.06$  and  $0.1$  was investigated. The high-purity precursor powders of  $SrCO_3$  (Sigma Aldrich, 98%),  $TiO_2$  (Sigma Aldrich, 99%),  $Pr_6O_{11}$  (Sigma Aldrich, 99.9%),  $NiO$  (Alfa Aesar, 99.9%) were weighted in the suitable stoichiometric molar ratio and put into the beaker with acetone. In the next step, the powders were stirred in ultrasonic bath in order to obtain a fine suspension of starting powders mixture. After the acetone has been evaporated, the powders of analyzed samples were transferred into the ceramic crucible and calcined at  $1000^\circ C$  for 10 h in air atmosphere. Next, obtained powders after calcination were milled in the ball mill for 12 h in isopropanol with zirconia balls ( $ZrO_2$ ), dried and uniaxially pressed into pellets. The sintering process of pellets was performed at  $1150^\circ C$ , for 10 h, also in air. The ex-solution process has been carried out 24 h at  $930^\circ C$  in dry  $H_2$  atmosphere ( $pO_2 \approx 10^{-25}$  atm.), in tubular furnaces under continuous flow ( $100 \text{ ml min}^{-1}$ ).

The crystal structure and phase composition of the grounded samples were analyzed using X-ray diffraction (XRD) performing on a Philips X'Pert Pro MPD with  $CuK_{\alpha 1}$   $\lambda = 1.54 \text{ \AA}$ . The microstructure of obtained samples was investigated by Scanning Electron Microscopy technique with a FEI Quanta FEG 250 with ET (Everhart–Thornley) secondary electron detector. The beam accelerating voltage was kept at 10 kV. In order to determine and confirm the initial stoichiometry of the sintered samples, the Energy Dispersive X-ray Spectroscopy (EDX) was performed by EDAX Genesis APEX 2i with ApolloX SDD spectrometer. The patterns obtained for the analyzed samples were analysed with Le Bail method. As an initial point, a unit cell constants of  $SrTiO_3$  tetragonal structure ( $I4/mcm$  SG) were used. The Pseudo-Voigt peak shape function was used in order to analyze and model the profile.

The magnetization measurements were carried out in Quantum Design PPMS (Physical Property Measurements System) using the ACMS susceptometry option at  $T = 293 \text{ K}$  in various magnetic field up to 3 T. The temperature dependence of total electrical conductivity was determined by conventional DC 4-wire method using the Keysight 34907A multimeter with an internal K-type thermocouple. The total conductivity measurements as a function of temperature were performed in a temperature range of  $100\text{--}800^\circ C$  at reducing atmospheres. The measurements with a four silver electrodes were performed at constant heating and cooling rates  $5^\circ C \text{ min}^{-1}$ . The redox cycles were conducted to check the chemical stability of Ni nanoparticles and reversibility of electrical conductivity values at  $800^\circ C$  in SOEC cathode/anode operating conditions. In this research redox cycles mean exposure material to oxidizing and reducing atmospheres alternately. One redox cycle can be described by following gas sequence: 2 h at 10%  $H_2$ -Ar ( $pO_2 \approx 10^{-26}$  atm.)  $\rightarrow$  1 h at Ar atmosphere ( $pO_2 \approx 10^{-6}$  atm.)  $\rightarrow$  2 h synthetic air atmosphere

( $p_{O_2} \approx 0.20$  atm.)  $\rightarrow$  1 h at Ar atmosphere ( $p_{O_2} \approx 10^{-6}$  atm.). After six full redox cycles material was exposed to pure, dry  $H_2$  atmosphere ( $p_{O_2} \approx 10^{-28}$  atm.) for 24 h.

### 3 Results and discussion

#### 3.1 Structural properties

In order to define the structure of the analyzed ( $Sr_{0.7}Pr_{0.3}Ti_{1-y}Ni_yO_3$ ) samples, the X-ray diffraction (XRD) measurements were done. XRD patterns of samples with different combinations of Ni dopant amount and A-site nonstoichiometry are presented in Fig. 1. As can be seen in Fig. 1a, in a stoichiometric sample ( $x = 1.0$ ) the cubic perovskite ( $Pr,Sr$ )(Ti,Ni) $O_3$  phase with a space group  $Pm-3m$  is predominant whereas in case of samples with nonstoichiometry in A site ( $x = 0.2$  and  $0.3$ ), a tetragonal perovskite phase with a space group  $I4/mcm$  was detected. This indicates that a nonstoichiometry in strontium sublattice affects a phase transition from cubic to tetragonal perovskite phase. Besides of this, some different secondary oxide phases were also detected in analyzed samples. In case of stoichiometric  $Sr_{0.7}Pr_{0.3}Ti_{0.94}Ni_{0.06}O_3$  sample a small amount of  $Pr_6O_{11}$  phase and some impurities which have no great influence on the structure can be visible. The  $x = 0.9$  sample was single-phase only with a small trace amount of  $Pr_6O_{11}$  phase, thus, it may be the optimal composition. In the sample with an  $x = 0.8$  A-site nonstoichiometry, a  $Pr_6O_{11}$  phase was not noticed, what indicate the higher stability of Pr-dopant. However, the higher nonstoichiometry level affects the presence of secondary  $TiO_2$  phase in the structure. The same effect was previously observed by Miruszewski et al. [18] in Y-doped  $SrTiO_3$ . Besides of this phase, the rhombohedral  $NiTiO_3$

oxide (space group  $R-3$ ) is also present in the sample. This indicates that reactivity of Ni-dopant with Ti-perovskite sublattice. It is worthy to underline that the amount of this phase is very low, thus, only a very small amount of nickel created the perovskite A-sublattice. The XRD results for samples with a higher Ni-dopant concentration in the structure are presented in Fig. 1b. As can be noticed, all samples have a very similar structure. The significant difference can be visible in case the presence of  $Pr_6O_{11}$  secondary phase. Now, the trace amounts are visible in all analyze compounds ( $x = 0.8-1.0$ ). Moreover, in the case of ( $Sr_{0.7}Pr_{0.3}Ti_{0.8}Ni_{0.1}O_3$ ) composition, the  $TiO_2$  phase is not observed. This may be caused by the higher Ni-dopant in the structure and in consequence the lower concentration of Ti in perovskite B-sublattice. The XRD patterns of the same chosen compound ( $Sr_{0.7}Pr_{0.3}Ti_{0.9}Ni_{0.06}O_3$ ) before and after the additional ex-solution process and also after the long redox cycle is shown in Fig. 2. The ex-solution process was performed as an additional isothermal heating at  $930$  °C in reducing atmosphere ( $H_2$ ), and redox cycle process was performed as six-time cycle of oxidizing the sample under oxygen condition and reducing in continuous  $H_2$  flow. As can be seen, no significant changes in the structure are visible. Only the tetragonal perovskite phase of doped  $SrTiO_3$  phase is visible which allows assuming the stability of material in the reduction–oxidation processes. It was also expected that the metallic nickel will be visible as an ex-solution product on the grain surfaces.

The Le Bail refinements for XRD pattern of samples: before and after ex-solution process as well as after several redox cycles were done. Refined unit cell parameters  $a$ ,  $b$ ,  $c$ , agreement indices  $R_{wp}$ ,  $R_{exp}$  and  $GOF$  are collected in Table 1.

As can be seen, the unit cell parameters of sample synthesized in air change after ex-solution process. In reduced

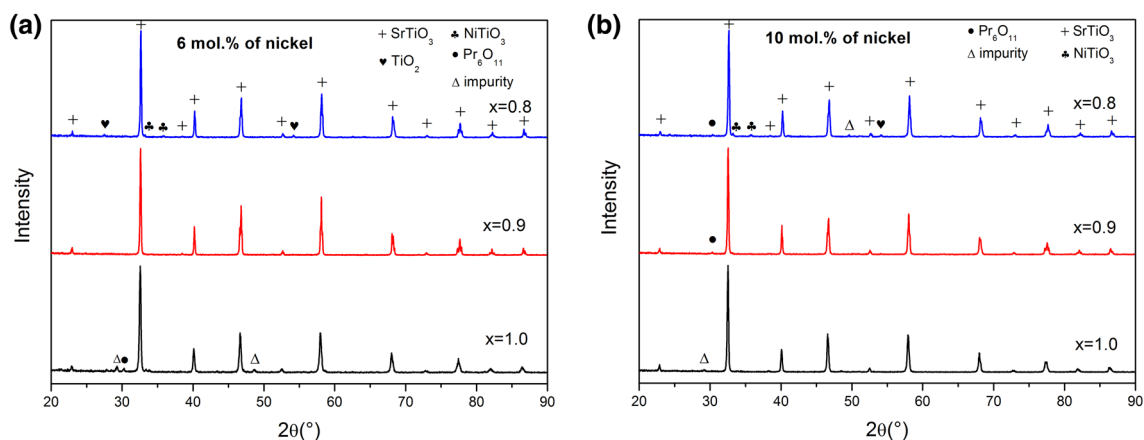


**Fig. 1** XRD patterns of ( $Sr_{0.7}Pr_{0.3}Ti_{1-y}Ni_yO_3$ ) samples sintered in air ( $p_{O_2} = 0.20$  atm.) at  $1150$  °C for 10 h, **a** 6 mol% of nickel dopant and different A-site nonstoichiometry ( $x = 1.0; 0.9, 0.8$ ) and **b** 10 mol% of nickel dopant and different A-site nonstoichiometry

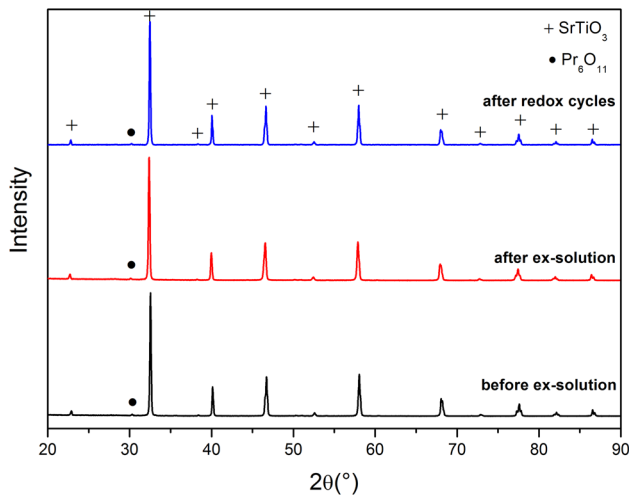


**Fig. 2** The results of XRD measurements of  $(\text{Sr}_{0.7}\text{Pr}_{0.3})_{0.9}\text{Ti}_{0.94}\text{Ni}_{0.06}\text{O}_3$  samples before and after ex-solution process and also after the redox cycles

**Table 1** Structural parameters of  $(\text{Sr}_{0.7}\text{Pr}_{0.3})_{0.9}\text{Ti}_{0.94}\text{Ni}_{0.06}\text{O}_3$  samples before and after ex-solution process and also after the redox cycles

	Before ex-solution	After ex-solution	After redox cycles
a (Å)	5.4997 (1)	5.4982 (1)	5.4987 (1)
b (Å)	5.4997 (1)	5.4982 (1)	5.4987 (1)
c (Å)	7.80568 (2)	7.8038 (1)	7.8035 (1)
R <sub>exp</sub> (%)	6.81	6.30	6.62
R <sub>wp</sub> (%)	11.73	9.93	12.06
GOF	2.96	2.48	3.31

atmosphere, a nickel cations as well as oxygen ions release the crystal lattice. Taking into account the observed decreasing of lattice constant it may be stated, that diffusion of Ni cations to the surface to Ni<sup>0</sup> forms has a major influence on lattice constant value. Moreover, the lattice constant hardly differs from each other after ex-solution and after redox cycles at 800 °C what is an expected behavior due to only a small change in the stoichiometry of the titanium and oxygen sublattice. The absence of Ni in the pattern probably indicates a very small amount of Ni in the analyzed specimen (possible nano-particles inclusions) and thus, it is below the accuracy of X-ray diffraction measurements.

### 3.2 Microstructure

The microstructure of prepared samples was investigated in order to analyze the influence of the composition on the porosity and average grain size. The obtained results are summarized in Table 2.

**Table 2** Porosities and grain sizes of different analyzed samples

Sample	Porosity [%] ± 2%	Average grain size [nm] ± 100 nm
$(\text{Sr}_{0.7}\text{Pr}_{0.3})_{0.8}\text{Ti}_{0.94}\text{Ni}_{0.06}\text{O}_3$	39	670
$(\text{Sr}_{0.7}\text{Pr}_{0.3})_{0.8}\text{Ti}_{0.9}\text{Ni}_{0.1}\text{O}_3$	34	940
$(\text{Sr}_{0.7}\text{Pr}_{0.3})_{0.9}\text{Ti}_{0.94}\text{Ni}_{0.06}\text{O}_3$	44	650
$(\text{Sr}_{0.7}\text{Pr}_{0.3})_{0.9}\text{Ti}_{0.9}\text{Ni}_{0.1}\text{O}_3$	41	890
$\text{Sr}_{0.7}\text{Pr}_{0.3}\text{Ti}_{0.94}\text{Ni}_{0.06}\text{O}_3$	62	210
$\text{Sr}_{0.7}\text{Pr}_{0.3}\text{Ti}_{0.9}\text{Ni}_{0.1}\text{O}_3$	59	380

It was expected that the Ni-metallic nanoparticles were exsolved from the oxide and cover the whole grain surface of materials. The microstructure of ceramics containing 6 mol% of Ni dopant and different nonstoichiometry level in A-sublattice (x = 1, 0.9 and 0.8) was shown in Fig. 3a–c respectively. Figure 3d–f presents the images for a sample with 10 mol% of Ni dopant. At first sight, the grain size of all samples was similar to each other besides the stoichiometric sample containing 6 mol% of Ni in Ti-sublattice (Fig. 3a). It seems, that a sintering temperature for the stoichiometric samples (x = 1.0) was too low. Nevertheless, a stoichiometric material containing a 10 mol% of nickel dopant (Fig. 3d) was mechanically more stable than ceramic containing 6 mol% of Ni in the structure. Concluding, nickel presence in the structure leads to the enhanced densifying of samples what provides more dense and mechanically more stable samples. This hypothesis was confirmed *i.a.* by porosity measurement. (see Table 2) The increased amount of Ni in the structure results in a decrease of sample porosity. It was also observed that a presence of nonstoichiometry in Sr-sublattice also leads to decrease of specimen's porosity. It is worthy to underline, that in the case of stoichiometric sample with 6 mol% Ni dopant, nanoparticles were not observed on the surface of the material's grains. Interestingly, a higher amount of nickel in titanium-sublattice induces the ex-solution process and small nanoparticles on the surface of grains can be observed. This shows that additional non-stoichiometry in the A-sublattice is not necessary provided that the amount of dopant will be appropriate.

It was expected that the non-stoichiometry and the higher nickel dopant would make the ex-solution effect will be more apparent. As can be seen, in three cases  $(\text{Sr}_{0.7}\text{Pr}_{0.3})_{0.9}\text{Ti}_{0.9}\text{Ni}_{0.1}\text{O}_3$ ,  $(\text{Sr}_{0.7}\text{Pr}_{0.3})_{0.9}\text{Ti}_{0.94}\text{Ni}_{0.06}\text{O}_3$  and  $\text{Sr}_{0.7}\text{Pr}_{0.3}\text{Ti}_{0.9}\text{Ni}_{0.1}\text{O}_3$ , nickel nanoparticles (< 50 nm) were homogeneously distributed over the whole grain surface. For the stoichiometric sample with 6 mol% Ni dopant, nanoparticles were not observed on the surface. Thus, increase of non-stoichiometry level to 20 mol% (x = 0.8) leads to creation of such a large amount Ni nanoparticles

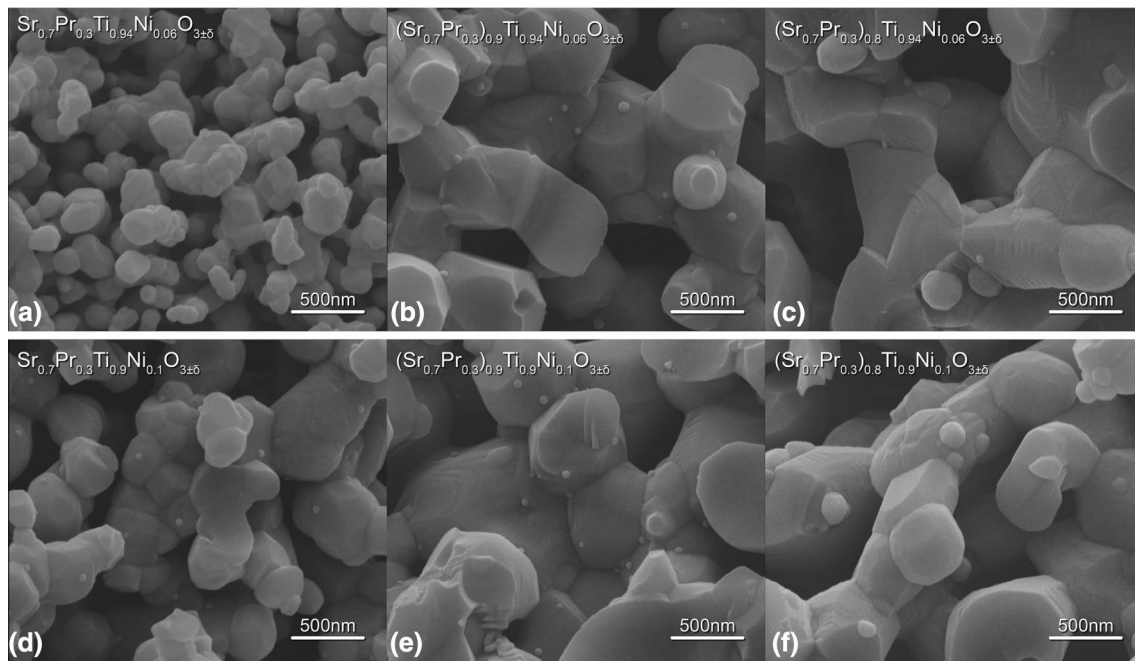


**Fig. 3** SEM images of  $(\text{Sr}_{0.7}\text{Pr}_{0.3})_{1-x}\text{Ti}_{0.94}\text{Ni}_{0.06}\text{O}_{3\pm\delta}$  samples after ex-solution process

that are merged into larger agglomerates with a diameter around 200–300 nm. Generally speaking, it is not a desirable effect. Based on these observations, the three compositions  $(\text{Sr}_{0.7}\text{Pr}_{0.3})_{0.9}\text{Ti}_{0.94}\text{Ni}_{0.1}\text{O}_3$ ,  $(\text{Sr}_{0.7}\text{Pr}_{0.3})_{0.9}\text{Ti}_{0.94}\text{Ni}_{0.06}\text{O}_3$  and  $\text{Sr}_{0.7}\text{Pr}_{0.3}\text{Ti}_{0.9}\text{Ni}_{0.1}\text{O}_3$  were chosen as a potential candidate for electrode support and that is why the electrical measurements were carried out on them. Figure 4 showed microstructure of  $(\text{Sr}_{0.7}\text{Pr}_{0.3})_{0.9}\text{Ti}_{0.94}\text{Ni}_{0.06}\text{O}_3$  before (Fig. 4a) and after (Fig. 4b) the ex-solution process and also after redox cycle (Fig. 4c). As can be seen, after synthesis in air there are not visible nanoparticles on the grain's surface. The observed porous microstructure was desirable to use that ceramic material as the electrode support in SOC devices. In the next step, the material was reduced,

and some of nanoparticles appeared on the whole grain surface (Fig. 4b). Sizes of these particles were smaller than ~50 nm and they were distributed homogeneously on the surface of grains. Subsequently, the material was exposed to reducing and oxidizing conditions. After six redox cycles, a cross-section of measured ceramic was investigated and shown in Fig. 4c. In this case, Ni nanoparticles were aggregated into agglomerates of ~200 nm diameter and the amount of ex-solved metallic nickel seems to be higher than in the analyzed sample before the few redox cycles. Concluding, created nanoparticles seem to be unstable and have a tendency to agglomerate after exposing sample on highly reducing and oxidizing atmospheres. Probably, the observed agglomeration of

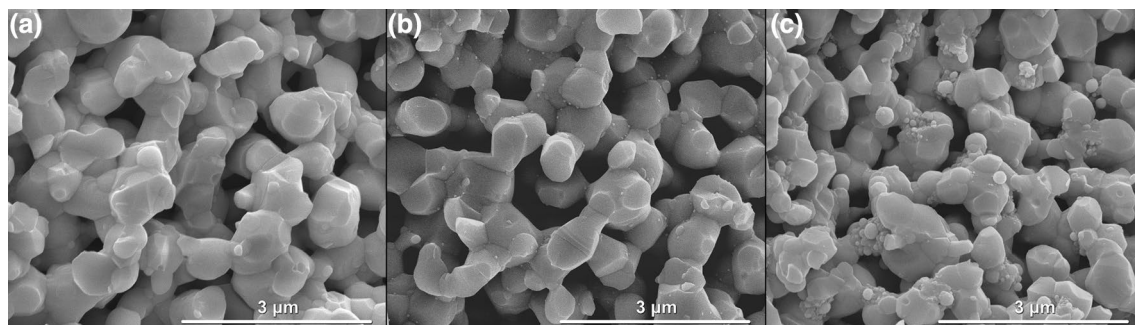


**Fig. 4** SEM images of  $(\text{Sr}_{0.7}\text{Pr}_{0.3})_{0.9}\text{Ti}_{0.94}\text{Ni}_{0.06}\text{O}_3$  sample **a** after sintered at 1150 °C **b** after ex-solution in reducing conditions, **c** after redox cycle

ex-solved nickel was caused by exposure of the material to oxidizing conditions during the cycling. Only just a part of Ni came back into the oxide bulk under oxidizing conditions, and therefore, the total Ni content on the surface can increase during the next redox cycle.

### 3.3 Magnetic properties

Quantitative estimation of the amount of nickel that was extracted from the structure in the ex-solution process was analyzed by field dependence of the magnetization. Measurements were performed for a material sintered at 1150 °C, after the ex-solution process and after the redox cycles. The ferromagnetic contribution of Ni particles to the total magnetization can be subtracted through the investigation of  $M$  vs  $H$  curves [19, 20]. The inset of Fig. 5a shows the experimental data ( $M_{\text{exp}}$ ) for three representative samples of  $(\text{Sr}_{0.7}\text{Pr}_{0.3})_{0.9}\text{Ti}_{0.94}\text{Ni}_{0.06}\text{O}_3$  measured at  $T=293$  K as a function of applied magnetic field ( $\mu_0 H$ ). For low magnetic field, the magnetization rapidly increases due to the presence of ferromagnetic Ni particles. It is noteworthy that the initial increase for the reference sample, with no visible particles of metallic Ni, is much weaker than for samples with Ni nanoparticles distributed on the grain's surface. For a magnetic field larger than the saturation field of elemental Ni, the magnetization curve  $M_{\text{exp}}(H)$  is a linear function of the applied magnetic field (solid line). This paramagnetic signal ( $M_{\text{para}}$ ) originates from the presence of praseodymium in the structure. The magnetization of Ni particles was then estimated by subtracting  $M_{\text{para}}(H)$  from the total magnetization  $M_{\text{exp}}(H)$  of the sample and results are shown in a main panel of Fig. 5a. The amount of elemental ferromagnetic Ni (here

given as a percentage of nominal Ni used for synthesis) was estimated from the saturation magnetization, assuming that for pure Ni  $M_s = 5.1 \times 10^5 \text{ A m}^{-1}$  [21]. As expected, the ferromagnetic signal ( $M_{\text{exp}} - M_{\text{para}}$ ) is the weakest for as prepared (sintered in air) material (open circles) amount of elemental nickel was estimated as 3.3%. For the sample after ex-solution processes and exposed to redox cycles estimated values were 14.1% and 14.6%, respectively. It is about four times larger than found for a reference sample. These results can be considered as evidence that during redox cycles there is a process of agglomeration but there is no increased amount of metallic nickel on the surface. The results of magnetic measurements showed also that only small amounts of nickel were ex-solved at grains surfaces in metallic form after reducing at low  $p\text{O}_2$ . So it can be stated, that a great part of Ni dopant is still incorporated in a Ti-sublattice as an acceptor dopant. Ni-dopant has, in this case, two functions—metallic form ( $\text{Ni}^0$ ) which may improve a catalytic activity and cationic-form in the structure ( $\text{Ni}^{2+}$ ) which can improve the ionic conductivity because of the ionic compensation of acceptor dopants by mobile oxygen vacancies.

In Fig. 5b a comparison of magnetization as a function of magnetic field measured for  $(\text{Sr}_{0.7}\text{Pr}_{0.3})_{0.9}\text{Ti}_{0.94}\text{Ni}_{0.06}\text{O}_3$  and  $(\text{Sr}_{0.7}\text{Pr}_{0.3})_{0.9}\text{Ti}_{0.9}\text{Ni}_{0.1}\text{O}_3$  samples after the ex-solution process is shown. As one can see, increase of the amount of nickel in the structure affect increases of the magnetization signal which is related to the increase in the amount of nickel nanoparticles on the grain surface. The quantitative estimation shows that in the case  $(\text{Sr}_{0.7}\text{Pr}_{0.3})_{0.9}\text{Ti}_{0.94}\text{Ni}_{0.06}\text{O}_3$  sample, a 14% of nickel is on the surface in a metallic form and for  $(\text{Sr}_{0.7}\text{Pr}_{0.3})_{0.9}\text{Ti}_{0.9}\text{Ni}_{0.1}\text{O}_3$  it is around 20%. This may strongly correspond to the

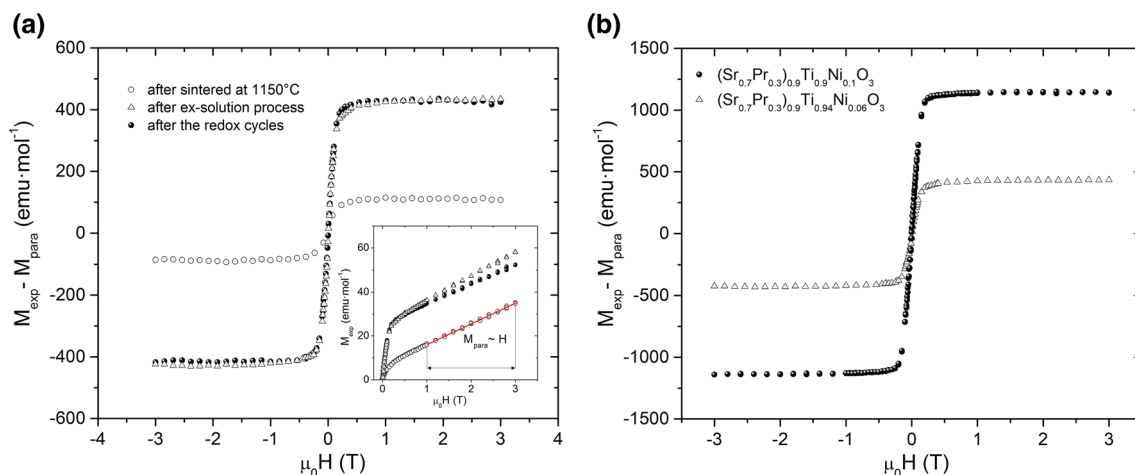


**Fig. 5 a** Magnetization as a function of magnetic field measured for  $(\text{Sr}_{0.7}\text{Pr}_{0.3})_{0.9}\text{Ti}_{0.94}\text{Ni}_{0.06}\text{O}_3$  sample before and after ex-solution. The additional result for a sample exposed to several

redox cycles was presented in the plot. **b** Magnetization as a function of magnetic field measured for  $(\text{Sr}_{0.7}\text{Pr}_{0.3})_{0.9}\text{Ti}_{0.94}\text{Ni}_{0.06}\text{O}_3$  and  $(\text{Sr}_{0.7}\text{Pr}_{0.3})_{0.9}\text{Ti}_{0.9}\text{Ni}_{0.1}\text{O}_3$  samples after ex-solution process

stoichiometry of materials:  $(\text{Sr}_{0.7}\text{Pr}_{0.3})_{0.9}\text{Ti}_{0.94}\text{Ni}_{0.05}\text{O}_3 + 0.01\text{Ni}^0$  and  $(\text{Sr}_{0.7}\text{Pr}_{0.3})_{0.9}\text{Ti}_{0.90}\text{Ni}_{0.08}\text{O}_3 + 0.02\text{Ni}^0$ , respectively. So, increase in the amount of nickel dopant, causes not only an increase in the amount of nanoparticles on the surface of grains but also amount of acceptor dopants in the structure.

### 3.4 Electrical properties

The electrical measurements of samples in which the formation of nickel nanoparticles was observed were performed using the DC-four wire method. Compositions with observed Ni nanoparticles:  $(\text{Sr}_{0.7}\text{Pr}_{0.3})_{0.9}\text{Ti}_{0.9}\text{Ni}_{0.1}\text{O}_3$ ,  $(\text{Sr}_{0.7}\text{Pr}_{0.3})_{0.9}\text{Ti}_{0.94}\text{Ni}_{0.06}\text{O}_3$  and  $\text{Sr}_{0.7}\text{Pr}_{0.3}\text{Ti}_{0.9}\text{Ni}_{0.1}\text{O}_3$ , were sintered in air ( $p\text{O}_2 \approx 0.20$  atm.) for 10 h at 1150 °C and reduced during ex-solution process in dry  $\text{H}_2$  ( $p\text{O}_2 \approx 10^{-25}$  atm.) for 10 h at 930 °C. Materials prepared in this way were used for electrical characterization. The temperature dependence of the total electrical conductivity in a function of  $1000/T$  for cooling regime is presented in Fig. 6. Analyzing the obtained results, it can be noticed that the introduction non-stoichiometry in A-sublattice significantly increases electrical conductivity. Additional, the slight effect of increasing the amount of nickel in the structure is observed. The conductivity of doped strontium titanate ceramics sintered in reducing atmosphere is considered to be mainly influenced by reduced  $\text{Ti}^{3+}$  cations concentration. The reduction of  $\text{Ti}^{4+}$  to  $\text{Ti}^{3+}$  introduces electrons into  $3d$  bands of  $\text{SrTiO}_3$ . Thus, the exposure of the analyzed samples to the low  $p\text{O}_2$  atmosphere increases the conductivity because the mentioned above electrons occupy the conduction band [22, 23]. It is worth noticing,

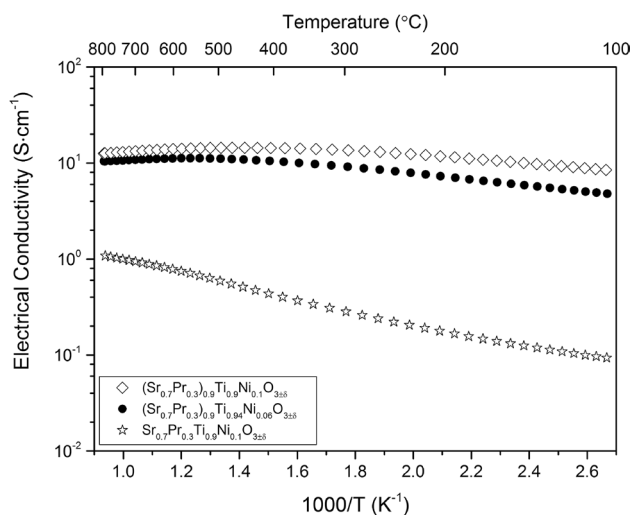


**Fig. 6** Electrical conductivity as a function of temperature for nanoparticle decorated samples sintered in air sintered in air ( $p\text{O}_2 = 0.20$  atm.) for 10 h at 1150 °C and reduced during ex-solution process in dry  $\text{H}_2$  ( $p\text{O}_2 = 10^{-25}$  atm.) for 10 h at 930 °C

that a transition from semiconducting-like to metallic-like behavior was observed for non-stoichiometry samples. This phenomenon may be explained by Mott's theory [24]. In the characteristic temperature, the concentration of delocalized electrons in the conduction band is much higher than thermally activated carries, and in this case this value starts to be independent on temperature and constant. At this moment the conductivity of material decreases in a function of temperature because of the decrease of electron mobility by a phonon scattering mechanism. As a consequence, the total conductivity at high operating temperatures slightly decreased above around 400 °C. In order to check the influence of the operating atmospheres on the electrical properties, chemical and mechanical durability and Ni-nanoparticles stability  $(\text{Sr}_{0.7}\text{Pr}_{0.3})_{0.9}\text{Ti}_{0.94}\text{Ni}_{0.06}\text{O}_3$  material was exposed on six redox cycles during a DC 4-wire experiment. In this case the gas change program and composition of the mixture during one complete cycle looked as follows: 2 h at 10%  $\text{H}_2$ -Ar ( $p\text{O}_2 \approx 10^{-26}$  atm.) → 1 h at Ar atmosphere ( $p\text{O}_2 \approx 10^{-6}$  atm.) → 2 h synthetic air atmosphere ( $p\text{O}_2 \approx 0.20$  atm.) → 1 h at Ar atmosphere ( $p\text{O}_2 \approx 10^{-6}$  atm.). Before first oxidizing and during the last reducing cycle, the same atmosphere like during ex-solution process was used—24 h in dry  $\text{H}_2$  ( $p\text{O}_2 \approx 10^{-28}$  atm.). It allowed observing the reversibility of the oxidation and reduction processes. The  $\sigma(t)$  results were presented in Fig. 7. For each cycle, when the ceramic was exposed to air atmosphere, a total conductivity significantly decreased by almost four orders of magnitude. This is related to the incorporation of oxygen into the structure and a reduction of oxygen vacancies concentration. Return of the system to the reducing atmosphere showed a slow increase of the total electrical conductivity close to the

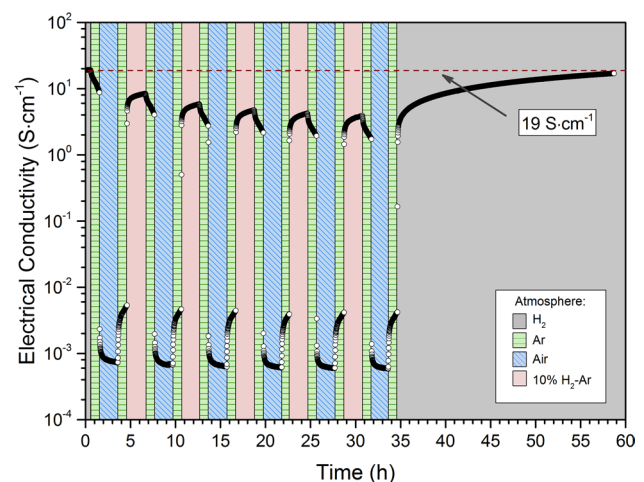


**Fig. 7** The total electrical conductivity of  $(\text{Sr}_{0.7}\text{Pr}_{0.3})_{0.9}\text{Ti}_{0.94}\text{Ni}_{0.06}\text{O}_3$  sample in a function of time during a redox cycles at 800 °C

level from the beginning of the measurement (before the oxidation). Results showed that the achievable value of conductivity under reducing conditions was  $19 \text{ S cm}^{-1}$ . Note that with each subsequent cycle the total electrical conductivity maximum was lower than in the previous one. After six cycles and after exposing the sample to dry  $\text{H}_2$  ( $p_{\text{O}_2} \approx 10^{-28} \text{ atm.}$ ) for 24 h, a total electrical conductivity came back to the level before the survey. Slow growth could be limited by a slow oxygen diffusion inside the material grains. Furthermore, the shape of the relaxation curves indicates that the expected high level of conductivity cannot be reached in a reasonable short time. Therefore, the material shows good chemical and mechanical stability under redox cycles. The total electrical conductivity changes were reproducible after six redox cycles and exposing the material to dry  $\text{H}_2$  atmosphere.

## 4 Conclusions

$(\text{Sr}_{0.7}\text{Pr}_{0.3-x}\text{Ti}_{1-y}\text{Ni}_y\text{O}_3$  with constant amount of 30% praseodymium dopant, different amount of nickel ( $y=0.06$  and  $y=0.10$ ) and additional nonstoichiometry in Sr-site ( $x=1$ ,  $x=0.9$  and  $x=0.8$ ) were investigated. The ex-solution of nickel nanoparticles was observed after a treatment of materials at reducing atmospheres and high temperatures. Additional non-stoichiometry ( $x=0.1$ ) in the A-sublattice facilitates this process, however, too large deviation from stoichiometry ( $x=0.2$ ) causes a presence of secondary  $\text{TiO}_2$  phase in the structure and formation of agglomerated grains in the ex-solution process. It was also shown, that nickel presence in the structure lead to the enhancement of the performance of densifying process what provides to the lowering of the sintering temperature. Magnetization measurement allowed to quantitative analysis of Ni nanoparticles. The results showed that only part of nickel diffuses onto the surface and Ni content on the surface does not change after redox cycle. An increasing amount of nickel dopant causes not only an increase in the amount of nanoparticles on the surface of grains but also amount of acceptor dopants in the structure. The studies of structural, magnetic and electrical properties of  $(\text{Sr}_{0.7}\text{Pr}_{0.3}\text{Ti}_{0.9}\text{Ni}_{0.06}\text{O}_3$  shown, that the proposed material can be considered as an electrode in SOFC/SOEC devices. The main problem that should be solved is the agglomeration of nickel nanoparticles into larger clusters, as has been observed in SEM images after several redox cycles. Moreover, it is necessary to check how the proposed material will behave in a complete SOFC/SOEC electrochemical device and how the specified amount of metallic Ni nanoparticles on the grain surface will improve the electrocatalysis in fuel cells.

**Acknowledgements** This work is supported by project funded by National Science Centre Poland based on decision Grant No. DEC-2015/19/D/ST8/02783.

## Compliance with ethical standards

**Conflict of interest** On behalf of all authors, the corresponding author states that there is no conflict of interest.

**Open Access** This article is distributed under the terms of the Creative Commons Attribution 4.0 International License (<http://creativecommons.org/licenses/by/4.0/>), which permits unrestricted use, distribution, and reproduction in any medium, provided you give appropriate credit to the original author(s) and the source, provide a link to the Creative Commons license, and indicate if changes were made.

## References

1. Jensen SH, Larsen PH, Mogensen M (2007) Hydrogen and synthetic fuel production from renewable energy sources. *Int J Hydrog Energy* 32:3253–3257
2. Holladay JD, Hu J, King DL, Wang Y (2009) An overview of hydrogen production technologies. *Catal Today* 139:244–260
3. Ebbesen SD, Jensen SH, Hauch A, Mogensen M (2014) High temperature electrolysis in alkaline cells, solid proton conducting cells, and solid oxide cells. *Chem Rev* 114:10697
4. Rossmeis J, Bessler WG (2008) Trends in catalytic activity for SOFC anode materials. *Solid State Ion* 178:1694–1700
5. Adijanto L, Padmanabhan VB, Gorte RJ, Vohs JM (2012) Polarization-induced hysteresis in CuCo-doped rare earth vanadates SOFC anodes. *J Electrochem Soc* 59:F751–F756
6. Madsen BD, Kobsiriphat W, Wang Y, Marks LD, Barnett SA (2007) Nucleation of nanometer-scale electrocatalyst particles in solid oxide fuel cell anodes. *J Power Sources* 166:64–67
7. Neagu D, Tsekouras G, Miller D, Menard H, Irvine JTS (2013) In situ growth of nanoparticles through control of non stoichiometry. *Nat Chem* 5:916–923
8. Nishihata Y, Mizuki J, Akao T, Tanaka H, Uenishi M, Kimura M, Okamoto T, Hamada N (2002) Self-regeneration of a Pd-perovskite catalyst for automotive emissions control. *Nature* 418:164–167
9. Yang L, Xie K, Xu S, Wu T, Zhou Q, Xie T, Wu Y (2014) Redox-reversible niobium-doped strontium titanate decorated with in situ grown nickel nanocatalyst for high-temperature direct steam electrolysis. *Dalton Trans* 43:14147–14157
10. Gao Y, Chen D, Saccoccio M, Lu Z, Ciucci F (2016) From material design to mechanism study: nanoscale Ni exsolution on a highly active A-site deficient anode material for solid oxide fuel cells. *Nano Energy* 27:499–508
11. Tanaka H, Uenishi M, Tanaguchi M, Tan I, Narita K, Kimura M, Kaneko K, Nishihata Y, Mizuki J (2006) The intelligent catalyst having the self-regenerative function of Pd, Rh and Pt for automotive emissions control. *Catal Today* 117:321–328
12. Madsen BD, Kobsiriphat W, Wang Y, Marks LD, Barnett SA (2007) SOFC anode performance enhancement through precipitation of nanoscale catalysts. *ECS Trans* 7:1339–1348
13. Katz MB, Zhang S, Duan Y, Wang H, Fang M, Zhang K, Li B, Graham GW, Pan X (2012) Reversible precipitation/dissolution of precious-metal clusters in perovskite-based catalyst materials: bulk versus surface re-dispersion. *J Catal* 293:145–148



14. Neagu D, Irvine JTS (2010) Structure and properties of La<sub>0.4</sub>Sr<sub>0.4</sub>TiO<sub>3</sub> ceramics for use as anode materials in solid oxide fuel cells. *Chem Mater* 22:5042–5053
15. Bochentyn B, Karczewski J, Miruszewski T, Krupa A, Gazda M, Jasinski P, Kusz B (2012) Donor-substituted SrTi<sub>1-x</sub>O<sub>3-δ</sub> anodes for SOFC. *Solid State Ion* 225:118–123
16. Yaremchenko AA, Patrício SG, Frade JR (2014) Thermochemical behavior and transport properties of Pr-substituted SrTiO<sub>3</sub> as potential solid oxide fuel cell anode. *J Power Sources* 245:557–569
17. Kamecki B, Miruszewski T, Karczewski J (2018) Structural and electrical transport properties of Pr-doped SrTi<sub>0.93</sub>Co<sub>0.07</sub>O<sub>3-δ</sub> novel SOEC fuel electrode materials. *J Electroceram*. <https://doi.org/10.1007/s10832-018-0143-0>
18. Miruszewski T, Bochentyn B, Karczewski J, Gazda M, Kusz B (2012) Microstructural and electrical properties of Y<sub>0.07</sub>Sr<sub>0.93-x</sub>TiO<sub>3</sub> perovskite ceramics. *Cent Eur J Phys* 10(5):1202–1209
19. Klimczuk T, Gupta V, Lawes G, Ramirez AP, Cava RJ (2004) Effect of Ru substitution for Ni on the superconductivity in MgCNi<sub>3-x</sub>Ru<sub>x</sub>. *Phys Rev B* 70:094511
20. Klimczuk T, Cava RJ (2004) The effect of Fe and Ru substitution on the superconductivity in MgCNi<sub>3</sub>. *Solid State Commun* 132:379–382
21. Callister WD Jr. (2007) *Materials science and engineering*. Wiley, New Jersey
22. Hui SQ, Petric A (2002) Electrical properties of yttrium-doped strontium titanate under reducing conditions. *J Electrochem Soc* 149:J1–J10
23. Huang X, Zhao H, Shen W, Qiu W, Wu W (2006) Effect of fabrication parameters on the electrical conductivity of Y<sub>x</sub>Sr<sub>1-x</sub>TiO<sub>3</sub> for anode materials. *J Phys Chem Solids* 67:2609
24. Mott NF (1968) Metal-insulator transition. *Rev Mod Phys* 40:677

**Publisher's Note** Springer Nature remains neutral with regard to jurisdictional claims in published maps and institutional affiliations.

